Available online at www.sciencedirect.com
SCIENCE DIRECT®
Journal of Magnetic Resonance 159 (2002) 226–236
JMR Journal of Magnetic Resonance
www.academicpress.com

Radical anions of fullerene bisadducts: a multifrequency CW-EPR study

Alfonso Zoleo,[a] Anna Lisa Maniero,[a,*] Marco Bellinazzi,[a] Maurizio Prato,[b] Tatiana Da Ros,[b] Louis Claude Brunel,[c] and Marina Brustolon[a]

[a] *Dipartimento di Chimica Fisica, Via Loredan 2, I-35131, Padova, Italy*
[b] *Dipartimento di Scienze Farmaceutiche, Università di Trieste, Piazzale Europa, I-34100 Trieste, Italy*
[c] *Center for Interdisciplinary Magnetic Resonance, National High Magnetic Field Laboratory, Florida State University, Tallahassee, FL 32310, USA*

Received 31 July 2002; revised 23 September 2002

Abstract

The radical anions of three C_{60} bisadducts (from now on termed CIS1, CIS2, and CIS3) have been studied in liquid solution and glassy matrix by X-band and high frequency CW-EPR spectroscopy. The three adducts CIS1, CIS2, and CIS3 are characterized by a pyrrolidinic ring and an isoxazolinic ring in position *cis*1-O, *cis*2-C, and *cis*3-C, respectively; the two rings are connected by a methylenic chain. In the X-band spectra of CIS1, one species has been observed showing hyperfine coupling constants with the pyrrolidinic nitrogen and ^{13}C nuclei, whereas in the X-band spectra of CIS2 and CIS3 more species are apparent, some with and other without hyperfine coupling with the pyrrolidinic ^{14}N. High field spectra at 110 and 220 GHz for all the bisadducts have been obtained; in all the cases, more species are evident with small differences in the *g*-factors. The occurrence of more species are discussed and put in relation with different bisadduct conformations. Furthermore, on the basis of the mechanism proposed for the ^{14}N hcc in previously studied fulleropyrrolidine (FP) monoanions, the presence or absence of ^{14}N hcc for CIS1 and the different conformations of CIS2 and CIS3 is discussed. The temperature dependence of the EPR linewidths and the *g*-factors of all the species have been determined and discussed in term of the different structural stiffness and symmetry of the three bisadducts.

Keywords: Fullerene anions; EPR; HF-EPR; Fullerene bisadducts; Multifrequency EPR

1. Introduction

The paramagnetic species produced by reduction of C_{60} and some of its derivatives have been extensively studied with EPR spectroscopy in the past years [1–15]. A comprehensive review on fulleride anions and fullerenium cations has been recently published [16].

An interesting class of fullerene derivatives is that of the fulleropyrrolidines (FP), prepared by 1,3-dipolar cycloaddition of azomethine ylides to C_{60} [17,18]. This methodology provides a broad variety of functionalized fullerenes, potentially useful for practical applications [19,20].

The present work complements our previous studies, [21,22], where we have shown that the EPR spectra of the radical anions of mono and bisFP give a good insight into their electronic structure. In fact in the case of FP radical anions the spectra show a hyperfine structure due to the interaction of the unpaired electron with the ^{14}N nucleus, and satellite lines due to the anions bearing a ^{13}C in some position of the bucky ball. From these data, we obtained useful information on the electron spin distribution of the π system and on its symmetry.

Moreover, the temperature dependence of the EPR linewidths and the direct measure of the spin–lattice relaxation time T_1 with pulsed EPR experiments have shown that the FP radical anions have in general a spin relaxation behaviour different from that of common radicals. T_1 is shorter than usual. This effect is known to be typical of fullerene derivatives: very short for C_{60}^- ($\sim$1 ns at room temperature), and then increasing in monoadducts

* Corresponding author. Fax: +39-049-8275135.
E-mail address: a.maniero@chfi.unipd.it (A.L. Maniero).

1090-7807/02/$ - see front matter © 2002 Elsevier Science (USA). All rights reserved.
PII: S1090-7807(02)00032-0

(for example ~100 ns for *N*-methylfulleropyrrolidine$^-$) and still increasing in bisadducts (~1 μs for bis-*N*-methyl-3,4-fulleropyrrolidine$^-$) but in any case shorter than in common radicals. Furthermore, the linewidths increase with increasing the temperature, and they depend on T/η, indicating a spin-rotational mechanism [22]. This effect is in some way anomalous for fullerenes, since it is normally important only for species much smaller, and actually, the spin-rotational mechanism was initially ruled out as a cause of the observed linewidths for the fullerene monoanions [23]. This latter conclusion was based on the hypothesis of a rigid rotor, assumption that is hardly acceptable for fullerene derivatives. As pointed out in [22], many different conformations for these species suggest a flexible structure, which can involve larger values of the spin-rotational coupling tensor. The interconversion among conformations can be the process that modulates the spin-rotational coupling affecting the T_1. The time modulation of spin–orbit interaction by the time fluctuation of orbital angular momentum can also affect the relaxation times with a T/η dependence [24]. This mechanism is effective only if the electronic states of the molecule are nearly degenerate, so that phonons of the solvent can excite radiationless electronic transitions: such a mechanism is probably effective for fullerene monoanions, where, as known, solvent phonons drive easy radiationless transitions between close electronic states related to slightly different conformations.

In either mechanism, conformational interconversion plays the main role in determining the relaxation rates.

Conformational changes can be constrained in bisadducts having a tether chain between the two addends. We have recently performed the cycloaddition of a nitriloxide to C_{60}, followed by the azomethine ylide generation, which attacks, within the same molecule, a second double bond of the same fullerene spheroid [25]. The isoxazoline and the pyrrolidine rings are linked by an aliphatic $(CH_2)_5$ arm. In this way, three positional isomers were obtained. The structure of the isomers has been determined by means of NMR spectroscopy [25] and is reported in Scheme 1 (bisadducts CIS1, CIS2, and CIS3) together with the structure of the symmetric bisadduct TRANS1 previously studied [26].

In the present work, we report an EPR study of the radical anions obtained by chemical reduction of these fullerene adducts. The presence of the methylene chain, which can be expected to increase the energy barrier between different conformations of the molecule, should lead to a decrease of the rate of interconversion between conformations.

By an X-band and High Frequency EPR (HF-EPR) study in liquid and solid solution, we show in this report that the radical anions of the bisadducts with the methylene chain are effectively present in several conformations. EPR spectroscopy allows the determination

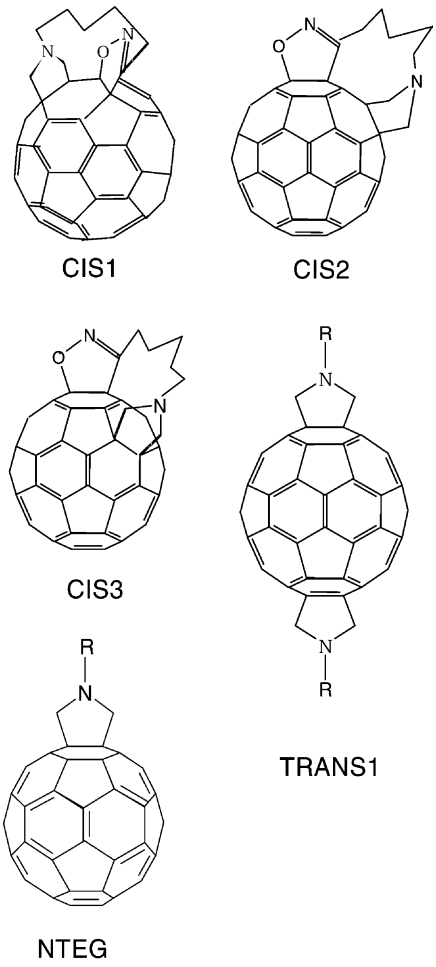

Scheme 1.

of the magnetic parameters of the different conformations, together with their concentrations.

Moreover, the number of the different conformations detected is different in X-band EPR and HF-EPR spectra, since it depends on the interconversion rate compared with the Larmor frequency difference between the various conformations. Very fast interconversion rates do not allow the observation of some conformations at X-band (10 GHz), while they are observed at W-band (100 GHz range).

2. Experimental

2.1. Instrumentation

X-band EPR measurements were performed with a computer controlled Bruker ER 200 D spectrometer, equipped with a nitrogen flow temperature controller. For *g* values calibration, the microwave frequency was measured with a 5342A Hewlett-Packard microwave

frequency counter and a LiTCNQ crystal was used as g value standard.

The HF-EPR spectra (around 110 and 220 GHz) were obtained at the NHMFL in Tallahassee (FL) with a home made spectrometer [27]. This machine is built around a superconducting magnet with a 17 T "main" coil and a ±0.1 T "sweep" coil (Oxford Instruments). The source which has been used in this work is a Gunn oscillator emitting in the 108–112 GHz range and equipped with a Schottky diode harmonic generator for obtaining higher frequencies (ABmm, Paris). The operating microwave frequency is measured with, and frequency locked to a source locking microwave counter (EIP 578B from EIP Microwave, Milpitas, CA).

The spectrometer was used in its basic configuration ("single pass" transmission mode), that uses oversized-cylindrical wave-guides for propagation of the microwave power. The transmission probe is in a liquid helium flow cryostat of the dynamic type (CF 1200 from Oxford Instruments); the temperature is monitored within ±0.1°. We used a liquid helium cooled In–Sb "hot electron" bolometer (QMC Instruments, Cardiff).

The spectra were obtained by modulation of the magnetic field at a frequency of 8 kHz with a modulation amplitude of 0.01–0.07 mT for spectra in liquid solution and of 0.2–0.5 mT for spectra in rigid phase. The main coil was in persistent mode and the magnetic field changed by variation of the additional field of the sweep coil.

2.2. Materials

Functionalized fullerenes considered in this paper are shown in Scheme 1 [25,26]. The following abbreviations are used for the compounds: CIS1, 1″,3′-pentan-4′*H*, 5′*H*-isoxazole[5′,4′:9,1]-pyrrolidin [3″4″:2,12] (C_{60}-I_h)[5,6] fullerene; CIS2, 1″,3′-pentan-4′*H*,5′*H*-isoxazole[5′,4′:1, 9]-pyrrolidin [3″4″:3,15] (C_{60}-I_h)[5,6]fullerene; CIS3, 1″, 3′-pentan-4′*H*,5′*H*-isoxazole[5′,4′:1,9]-pyrrolidin [3″4″:13, 14] (C_{60}-I_h)[5,6]fullerene; NTEG, *N*-(3,6,9-trioxadecyl)-3,4-fulleropyrrolidine (1′,5′-dihydro-1′-[2-[2-(2-methoxyethoxy)ethoxy]ethyl]-2′*H*-[5,6]fullereno-C_{60}-I_h-[1,9-c] pyrrole); TRANS1, bis-TRANS1-[*N*-(3,6,9-trioxadecyl)-3,4]-fulleropyrrolidine.

Dibenzo-18-crown-6 ether was used as purchased from Aldrich. 2-Methyltetrahydrofuran (MeTHF) was distilled over sodium before use.

2.3. Anion preparation

The very same samples of the CIS1, CIS2, and CIS3 monoanions were used for both X-band and W-band EPR spectroscopy.

The radical anions were prepared by standard vacuum (10^{-4} mbar) techniques in a 10 mm o.d. Pyrex tube. The tube was equipped with three lateral arms. The first one contained the fullerene sample together with the dibenzo-18-crown-6 ether in equimolar amount. In the second one a sodium mirror was formed by evaporating the pure metal from a sodium-filled Drummond calibrated capillary, before introducing the solvent through the vacuum line. The third arm was equipped with a usual quartz EPR tube. After preparation of the sample solution according to the procedure described in [21], a small amount of this solution was transferred in the EPR tube that was sealed with a flame and removed from the remaining apparatus: in this way the EPR tube with the sample is kept permanently under vacuum, and no step occurs where the sample is exposed to air.

The concentrations of the samples were 10^{-5} M.

3. Results

3.1. CW X-band EPR of CIS1

The spectra recorded at different temperatures in liquid solution of MeTHF are reported in Fig. 1. They show the hyperfine structure due to the coupling with one ^{14}N nucleus. The hyperfine coupling constant (hcc) is reported in Table 1, where we report also the ^{14}N hccs of other FP anions for comparison. It should be noted that the present radical has a ^{14}N hcc which is nearly one-half of the hcc of other fulleropyrrolidines.

In Fig. 2 an experimental spectrum, expanded to show the hyperfine structure of the satellite lines due to radicals bearing a ^{13}C nucleus, is shown together with its simulation. The simulations were obtained on the basis of a best fit procedure by varying the number of different ^{13}C hyperfine couplings, the relative abundance of the radicals bearing each type of coupled ^{13}C nucleus, and the values of the hyperfine coupling constants. The results are reported in Table 2. All the radicals bearing a ^{13}C are present with the abundance of 1%, indicating

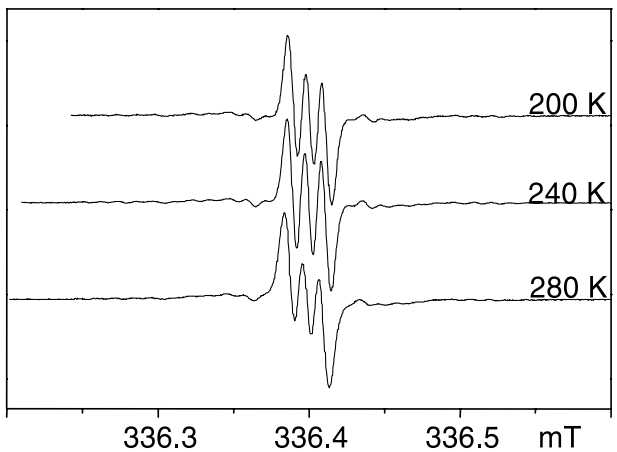

Fig. 1. X-band CW-EPR spectra of CIS1 monoanion in MeTHF.

Table 1
^{14}N hyperfine coupling constants for some fulleropyrrolidine radical anions

	CIS1[a]	CIS2[a]	CIS3[a]	NTEG[b]	TRANS1[b]	MFP[c]	TegMFP[c]	bisNMP[c,d]
^{14}N hcc	0.011	0.021 (I) 0.0 (II) 0.027 (III) 0.023 (IV)	0.022 (III) 0.000 (II) 0.000 (I)	0.022	0.021	0.022	0.023	0.021 0.025

The values (obtained from X-band EPR) are in mT. Precision $\pm 10^{-3}$ mT.
[a] This work.
[b] Ref. [22].
[c] Ref. [21].
[d] Two radicals were observed.

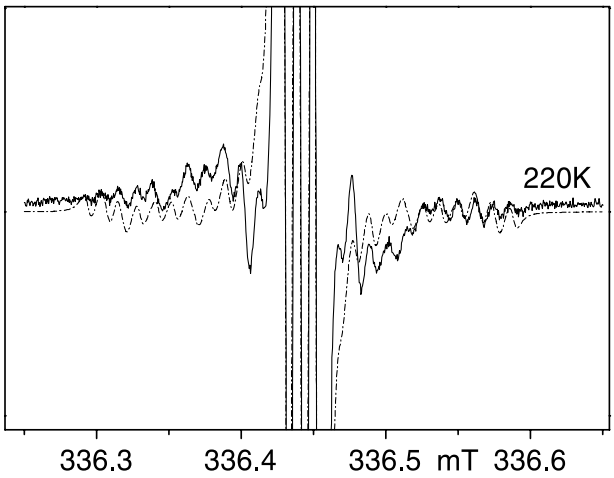

Fig. 2. Expanded view of the X-band spectrum of CIS1 monoanion in MeTHF at 220 K with simulation.

that there are not equivalent positions, as expected because of the radical symmetry.

On decreasing the temperature from 280 K the EPR linewidths decrease until 220 K, then increase again on further lowering the temperature. The linewidths at different temperatures are reported in Table 3.

The *g*-factor is 2.0001, a typical value of a fullerene radical anion.

3.2. CW X-band EPR of CIS2

Fig. 3 reports the X-band EPR spectra of CIS2 radical anion at three temperatures.

The quite complex pattern can be ascribed to the presence of at least four different species, three of them showing ^{14}N hyperfine splitting (Table 1). The simulation (Fig. 4) of the best resolved spectrum at 160 K allows the determination of the *g*-factors and the ^{14}N hccs of the four radicals.

The *g*-factors, the linewidths, and the relative concentrations of the four radicals at different temperatures are reported in Table 4. For three of the species (II, III, and IV) there is a very slight increase of the linewidths on increasing the temperature. The relative concentrations of the radicals vary with the temperature indicating equilibrium between them. The species lacking the ^{14}N coupling (species II) is always present with the highest concentration.

3.3. CW X-band EPR of CIS3

The spectra at different temperatures in liquid solution of MeTHF are reported in Fig. 5.

The spectra show the presence of three radicals: two give a single line spectrum (species I and II in Fig. 5) and

Table 2
^{13}C hyperfine coupling constants (in mT, precision $\pm 10^{-3}$ mT) and abundance (%) of radicals bearing one ^{13}C for CIS1, NTEG, and TRANS1 monoanions (from simulations of the X-band EPR spectra)

CIS1	^{13}C hcc	0.272	0.244	0.174	0.122	0.076	0.054
	Abundance (%)	1	1	1	1	1	1
NTEG	^{13}C hcc	0.200	0.165	0.112	0.070		
	Abundance (%)	2	2	4	4		
TRANS1	^{13}C hcc	0.176	0.046				
	Abundance (%)	4	8				

Table 3
Linewidth (LW) at different temperatures of CIS1 monoanion (from simulations of the X-band EPR spectra)

LW	8×10^{-3}	7×10^{-3}	6×10^{-3}	6×10^{-3}	7×10^{-3}	7×10^{-3}
Temp.	180 K	200 K	220 K	240 K	260 K	280 K

Linewidth are in mT (prec. err. $\pm 10^{-3}$ mT).

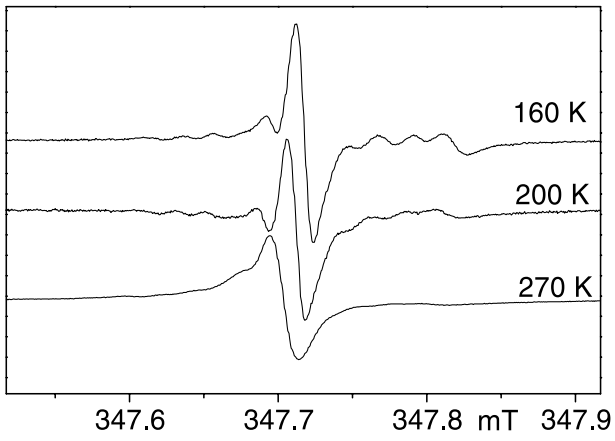

Fig. 3. X-band spectra of CIS2 monoanion in MeTHF.

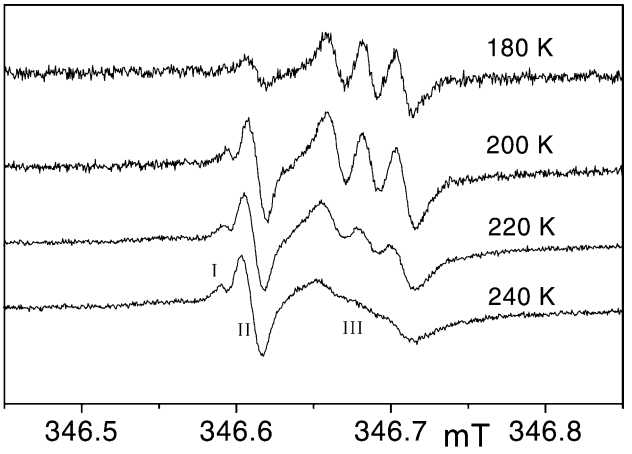

Fig. 5. X-band spectra of CIS3 monoanion in MeTHF.

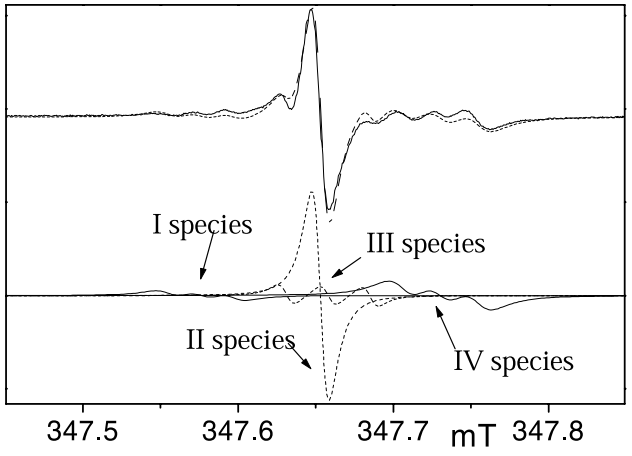

Fig. 4. Spectrum of CIS2 monoanion together with simulation (dotted line) at 160 K. Below, the reconstruction of the simulation shows the features due to the four species underlying.

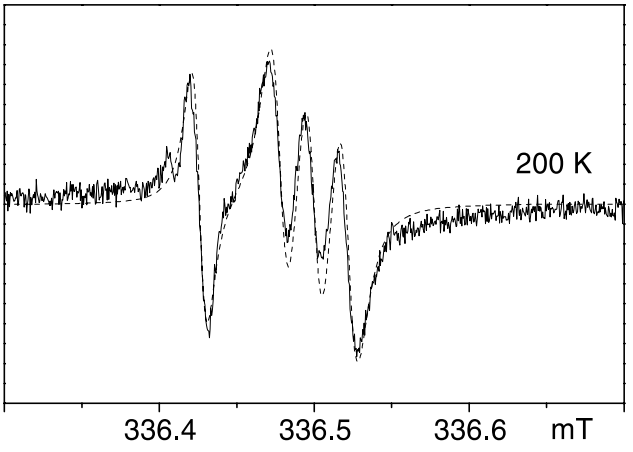

Fig. 6. X-band spectrum of CIS3 monoanion at 200 K with simulation (dotted line).

the third one a triplet spectrum due to the coupling with a ^{14}N nucleus (species III). In Fig. 6 the spectrum at 200 K is reported along with its simulation, from which the ^{14}N hcc of the species III (Table 1) and the *g*-factors of the three radicals (Table 5) have been determined. Table 5 reports also the linewidths and the relative concentrations of the three species at different temperatures.

3.4. High Frequency EPR spectra of CIS1

In Fig. 7, we report the W-band EPR spectra, recorded at about 110 GHz, at different temperatures. At low temperature the glassy phase spectrum has a total width of about 1.5 mT and shows features indicating the superposition of different species with different *g*-tensors.

On increasing the temperature, the spectrum narrows as the solvent softens and at 210 K four narrow lines

Table 4
Linewidth (LW), *g*-factors, and relative concentrations (RC) of the four species of CIS2 monoanion (from simulations of the X-band EPR spectra)

Species	I		II		III		IV	
g-Factors	2.0012 ± 0.0001		2.0008 ± 0.0001		2.0007 ± 0.0001		2.0003 ± 0.0001	
Temp.	LW	RC	LW	RC	LW	RC	LW	RC
240 K	0.015	6%	0.016	64%	0.014	6%	0.025	24%
220 K	0.015	5%	0.014	80%	0.011	5%	0.025	12%
160 K	0.018	2%	0.011	79%	0.011	9%	0.021	10%

Linewidths are in mT (prec. err. $\pm 10^{-3}$ mT) and relative concentrations are expressed as percentage of the total intensity (rel. err. 5%).

Table 5
Linewidth (LW) and relative concentrations (RC) for the three species of CIS3 monoanion (from simulations of the X-band EPR spectra)

Species	I		II		III	
g-Factors	2.00034 ± 0.00010		2.00030 ± 0.00010		2.00010 ± 0.00010	
Temp.	LW (mT)	RC	LW (mT)	RC	LW (mT)	RC
180 K	—	—	0.010	11.0%	0.010	89.0%
200 K	0.004	1.0%	0.009	12.9%	0.011	86.1%
220 K	0.005	0.9%	0.007	12.6%	0.017	86.5%
240 K	0.007	1.6%	0.009	12.4%	0.022	85.6%

Linewidths are in mT (prec. err. $\pm 10^{-3}$ mT) and relative concentrations are expressed as percentage of the total intensity (rel. err. 5%).

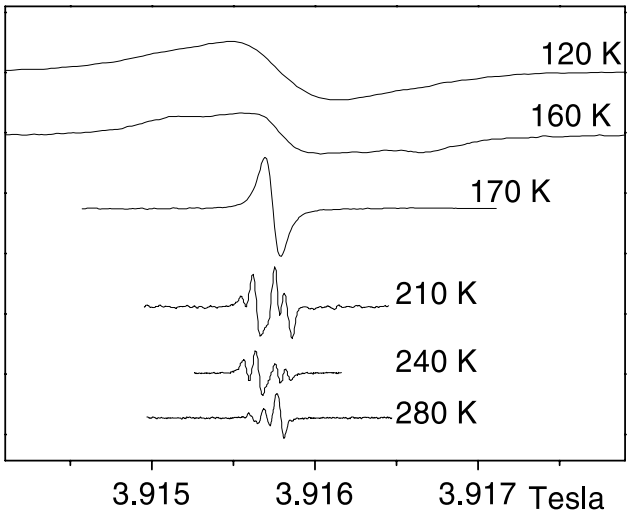

Fig. 7. W-band spectra of CIS1 monoanion in MeTHF.

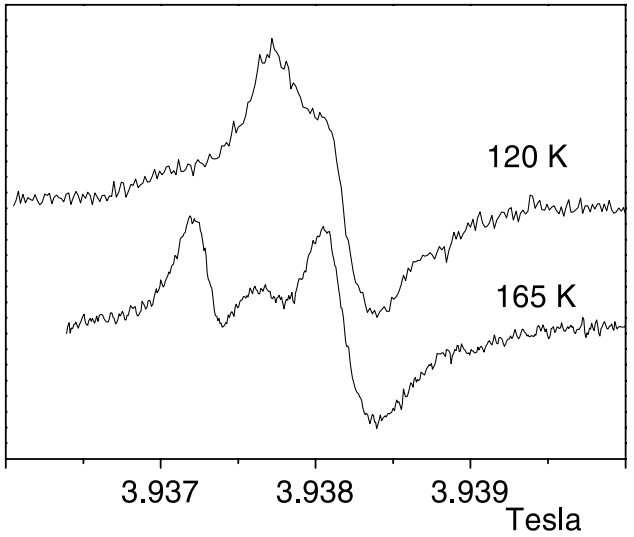

Fig. 8. W-band spectra of CIS2 monoanion in MeTHF.

(linewidth about 0.05 mT) appear. On varying the temperature, the relative intensities of the lines vary. Moreover, different experiments with the same sample at the same temperature but with different thermal approaches give rise to slightly different relative intensities of the lines. The difference in the *g*-factors between the first and fourth line is $\Delta g_{\max} \approx 1.3 \times 10^{-4}$.

3.5. High Frequency EPR spectra of CIS2

In Fig. 8 the W-band spectra recorded at 120 and 165 K of CIS2 are presented. Although the EPR tubes were carefully sealed, minute leaks led to a degradation of the samples. Because of this degradation, it was not possible to acquire W-band spectra in the full temperature range. In our opinion it is of paramount importance to use the same bisadduct derivatives to prepare the anions used for all the spectroscopic measurements. The limited temperature range available for the W-band measurements does not restrict the analysis of the data. For instance, the W-band spectra at 120 and 165 K illustrate very clearly the passage from a frozen matrix (120 K) to almost a fluid solution (165 K): the inhomogeneously broadened spectrum at 120 K changes to a more resolved spectrum at 165 K. The lines (linewidths 0.2–0.4 mT) in the 165 K spectrum can be attributed to at least three different species.

The low resolution of this high field spectrum does not allow a clear correlation between the species detected at X- and W-bands. Nevertheless, the $\Delta g_{\max}$ at W-band is about 4.5×10^{-4}, which compares well with the difference in *g*-factors between the species II and IV seen in the X-band spectra. The species I shows very low intensity at X-band and is not visible at high frequency.

3.6. High Frequency EPR spectra of CIS3

The W-band spectra in liquid solution clearly show the presence of four species (Fig. 9). In the spectrum at 180 K the linewidths of the four species are about 0.15 mT and $\Delta g_{\max} \approx 6.5 \times 10^{-4}$. The difference in the *g*-factor of the two more intense species is $\Delta g \approx 1.9 \times 10^{-4}$: this difference agrees with the *g*-factor difference between the species II and III, which are the only species visible at 180 K in the X-band spectrum. The species I is visible in X-band only for $T > 200$ K and has a *g*-factor that does not fit either of the low field feature in the W-band spectrum at 180 K.

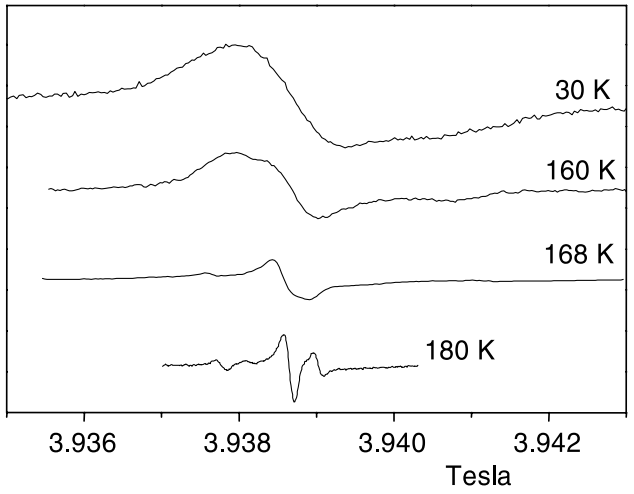

Fig. 9. W-band spectra of CIS3 monoanion in MeTHF at different temperatures.

In frozen matrix the spectra become very broad: the total linewidth is about the double of the linewidth observed in the CIS1 and CIS2 bisadduct spectra. This feature is clearly evident in Fig. 10, where the glassy phase spectra recorded at 220 GHz of the three CIS bisadducts are reported. For comparison in the same figure the spectrum of a symmetric FP bisadduct is reported from [22].

4. Discussion

4.1. General features of the X-band and High Frequency EPR spectra and g-factors

X-band EPR spectra of mono and bisFP radical anions show generally a single species having

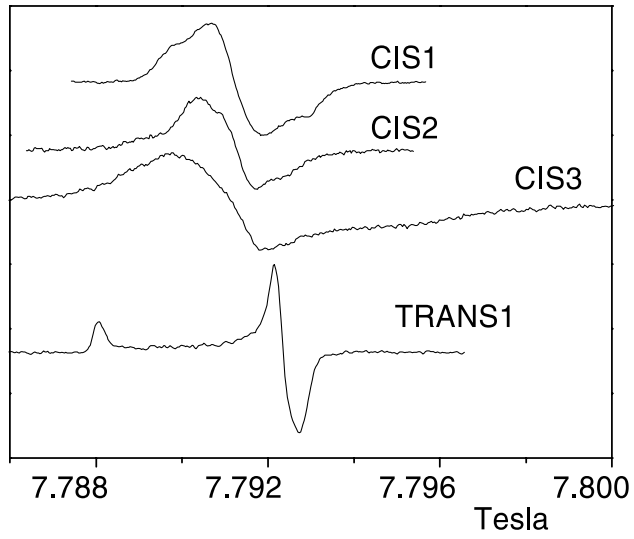

Fig. 10. Spectra at 220 GHz in glassy phase of the CIS adducts. The glassy phase spectrum of TRANS1 at 220 GHz [22] is shown for comparison.

hyperfine coupling with the pyrrolidinic nitrogen and satellite lines due to ^{13}C hyperfine structure [21,22]. The anomalous temperature dependence of the EPR linewidths of the latter radical anions was explained as due to a fast averaging between different conformations.

This rapid interconversion was related to quick radiationless transitions between nearly degenerate electronic states affecting the relaxation times. In agreement with this hypothesis, we have shown that for different bisadducts the anomalous contribution to the electron spin relaxation behaviour decreases [22] as the stiffness of the fullerene moiety and therefore the conformational energy difference increase. We have proposed that the rapid interconversion among different conformations and the related fast radiationless transitions between the electronic states modulate the spin-rotational and spin–orbit interactions in the spin hamiltonian, which appears to be responsible for the short relaxation times [22].

The detection of different conformations depends upon the rate of the interconversion, compared with the difference between the resonance frequencies of the EPR lines of the different radicals. For example an interconversion between conformations with no difference in the Zeeman energy and in the ^{14}N hccs, but large enough differences in the ^{13}C hccs, could give rise to a broadening of the ^{13}C satellite lines, leaving the shape of the main spectrum unchanged. This would be the case for example of a dynamical Jahn–Teller effect leading to interconversion between several equivalent conformations with the same g value and ^{14}N hcc, but in which the ^{13}C nuclei would be exchanging their different hccs.

The radical anions studied in this paper lack any symmetry element, and therefore we expect that their different conformations should correspond also to different g-factors, and different ^{14}N hccs. In fact the spectra of CIS1, CIS2, and CIS3 show the presence of several radical anions with very small differences in g-factors and some of these radicals show different hccs with the ^{14}N nucleus.

In the case of CIS2 and CIS3, the presence of several radicals is detectable both in X-band and W-band EPR spectra, whereas in the case of CIS1 the small differences in the g-factors do not allow to disentangle their features in the X-band spectra. This latter compound has two nearby rings, connected by a floppy aliphatic chain. A quite flexible structure results that allows several conformations with little energy differences. Actually, four species are observed at W-band (Fig. 7), with intensity ratios changing with the temperature and thermal approach, which strongly supports the hypothesis of interconverting conformers. Only one species is visible in X-band spectra (Figs. 1 and 2), because the low energetic barrier between the conformations

leads probably to a rapid interchange on the X-band timescale.

In CIS2 and CIS3, the rings are bonded further apart to the buckyball, which induces a strain in the aliphatic chain and an increased rigidity of the fullerenic sphere. In this case, the higher conformation energy barrier involves well-separated conformations and effectively different species are observed even in the X-band spectra (Figs. 3–6).

The occurrence of several conformations for the CIS adducts can be also inferred by comparing the lineshapes of their glassy phase HF-EPR spectra, recorded at 220 GHz, with the spectrum obtained for the more rigid and symmetric FP bisadduct TRANS1 (see Fig. 10). In [22] we obtained that TRANS1 is present, both in solution and in glassy phase, in a single conformation. From the simulation of the well-resolved glassy phase HF-EPR spectrum, it was possible to determine the principal components of the quasi-axial g-tensor. The 220 GHz unresolved rigid spectra of the CIS bisadducts are clearly due to many conformers with different, but close and slightly anisotropic g-tensors. CIS1 and CIS2 gave in fact narrower powder spectra with respect to TRANS1. The HF-EPR spectrum of CIS3 adduct is much broader, probably because its different conformations have larger differences in the g-tensors, as the conformations detected in the liquid phase HF-EPR spectra show larger differences in the g-factors (for CIS1 and CIS3 conformers $\Delta g_{\max} \approx 1.3 \times 10^{-4}$ and 6.5×10^{-4}, respectively, that correspond, at 220 GHz, to $\Delta B_{\max} \approx 0.5$ and 2.5 mT).

The g-factor values for all the species are largely below the free electron g-factor value and this is a well-known feature of fullerene anion derivatives. Although a clear theory is not yet available to explain fully the low g values, authors agree that this fact is due to the closeness of the electronic states in these species [2,5]. We have shown in our previous reports that the fullerene derivative g-factor values are shifted toward higher values with respect to the C_{60} g-factor according to a lower symmetry and/or a higher structural stiffness [22]. So g-factors can be used as a rough estimate of the structural features of a fullerene derivative radical anion.

The single species in the X-band spectra of CIS1 exhibits a $g = 2.0001$, very close to 2.0000, and the species observed at high frequency have g-factors differing from this value of less than $\pm 1 \times 10^{-4}$.

This means that the Zeeman frequencies of the different species observed at W-band have differences of the order of $\sim 3 \times 10^6\,s^{-1}$; the difference at X-band would be 10 times smaller, $\sim 3 \times 10^5\,s^{-1}$. Since at W-band the different species are detectable, whereas at X-band they give rise to a single line, we must conclude that the interconversion frequency is between these two values.

In CIS2 and CIS3 spectra the g values obtained from the X-band spectra are larger than 2.0001 for most of the species, indicating a shift toward higher values according to the increased stiffness.

4.2. ^{14}N hyperfine couplings

In Table 1 we report the ^{14}N hyperfine couplings for our CIS adducts together with the hccs of other fulleropyrrolidine mono- and bisadducts. It is worth to note that for all species the ^{14}N hccs are very similar except for CIS1. Apart from CIS1, for all species the ^{14}N hcc value is about 0.02 mT. Since it is well known that the spin density is mainly located on the equatorial belt of the fullerene sphere [12,13], the hyperfine coupling with the ring nitrogens requires a through bond spin polarization or a direct spin-density transfer toward the nitrogen nuclei.

In our previous report [21], we ruled out the spin polarization mechanism as a source of coupling, on the basis of the too large ^{14}N hyperfine constant, and showed that a direct spin-density transfer from the π distribution to the sp^3 lone pair was instead fully consistent with this value. Furthermore, this mechanism, called *periconjugation*, has been already mentioned in the literature to explain other effects [28,29].

According to the model of the periconjugation, the nearest carbon atoms having spin density (carbons 3a, 3b in Fig. 11a) overlap their p orbitals with the lone pair sp^3 orbital of the pyrrolidinic nitrogen. In order to have effective interaction, the ring has to be bent toward the sphere, i.e., the molecule has to assume the shown conformation. In Fig. 11b, we report the same conformation for CIS1, which is the only adduct (among the ones we studied) where the carbon position 3b is occupied by the isoxazolinic ring. Therefore, only one carbon p orbital is available for the spin-density transfer, and not surprisingly, the ^{14}N hyperfine coupling constant is one-half of the usual ones (0.011 mT instead of 0.02 mT).

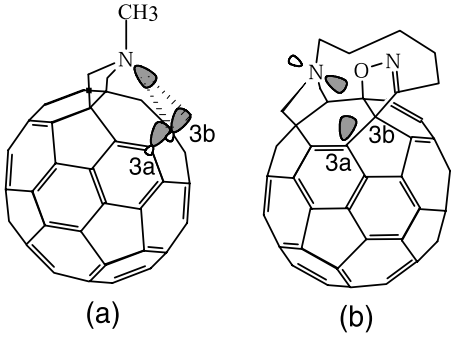

Fig. 11. (a) Theoretical model of periconjugation, invoked to explain the observed ^{14}N hyperfine coupling constant in NMP monoanion [21]. (b) The same model for CIS1: only one carbon p orbital in position 3a can interact with the lone pair sp^3 nitrogen orbital.

For CIS2 and CIS3, several species can be observed in the spectra, some with and some without ^{14}N hyperfine coupling. According to our model only conformations with the pyrrolidinic ring bent toward the sphere have the proper geometry to give rise to the hyperfine interaction. We can assume that the strain of the aliphatic chain in CIS2 and CIS3 allows for conformations where the nitrogen lone pair orbital points away from the fullerenic sphere, as shown for CIS2 in Fig. 12, which results in conformers without ^{14}N hyperfine coupling.

We can notice also that the isoxazolinic nitrogen does not seem to interact with the fullerenic sphere, or at least does not give a measurable constant. We can rule out that the observed nitrogen hcc in the CIS adducts is due to the isoxazolinic instead of pyrrolidinic nitrogen, since the adducts containing only the pyrrolidinic ring (see Table 1) do show the same hyperfine coupling. The nitrogen hccs we observe have been rationalized in terms of a direct spin transfer [21] and DFT-type studies were presented in [22].

4.3. ^{13}C hyperfine couplings

In the X-band EPR spectra of CIS1 satellite lines beside the central triplet are apparent. These lines are due to radicals with one ^{13}C in some position of the buckyball and this coupling can be very useful to investigate the spin distribution on the fullerene sphere of the FP adducts. From the simulations of the CIS1 spectra, we obtain six sets of hccs, each set containing only one radical. The number of sets is an indication of the non-equivalent carbon positions on the buckyball.

By comparison, in Table 2 we show the ^{13}C hyperfine couplings for the two FP adducts studied in [22], TRANS1$^-$ and NTEG$^-$. Both TRANS1$^-$ and NTEG$^-$ hccs involve 12 carbon atoms, but in TRANS1$^-$ they are grouped in two sets, while in NTEG$^-$ they are in four sets. The number of carbons, which hyperfine coupling constants could be measured for, is 6 in CIS1$^-$. This can be explained, assuming that in CIS1$^-$ several carbon atoms have a very low spin density and the radicals with a ^{13}C in these positions are unable to give detectable ^{13}C hyperfine couplings in the CW-EPR spectra. Furthermore, the six carbon atoms are grouped in six different sets. This means that the symmetry of spin distribution decreases in the order: TRANS1$^-$, NTEG$^-$, and CIS1$^-$.

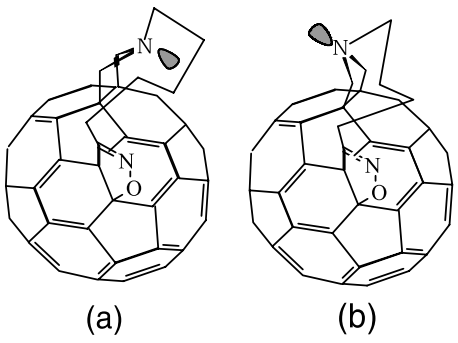

Fig. 12. Possible conformations of CIS2 with the nitrogen lone pair orbital pointing toward the fullerenic sphere (a) and far from the fullerenic sphere (b).

4.4. CW-EPR linewidth

The EPR linewidths of radicals in dilute solutions are determined usually to large extent by modulation of the anisotropic parameters in the Hamiltonian: the source of this modulation is commonly rotational diffusion. For rotational correlation times typical of medium-sized radicals in low viscosity solutions, only secular and pseudosecular contributions to the electron spin relaxation need to be taken into account in the X-band EPR spectroscopy. In this motion regime, the spin–lattice relaxation time T_1 is longer than the spin–spin relaxation time T_2 and the linewidth increases on increasing solution viscosity, i.e., lowering temperature [30].

On the other hand, it is well known that the EPR spectra of C_{60} monoanion consist of a single broad line at room temperature, which strongly narrows on decreasing temperature [2,5,6]. This anomalous behavior has been widely discussed in the past years and authors generally agree that it depends on non-secular contributions, responsible for unusually short spin–lattice relaxation times [5,23,31]. A similar trend of the linewidths, though less pronounced, is displayed by several FP radical anions, which we have studied in our previous reports. In these cases, the T_1 times were measured directly by saturation and inversion recovery pulse techniques and resulted very short if compared with the T_1 relaxation time of TRANS1 monoanion, which did not show anomalous linewidth trend. In these cases, T_1 was actually determining the CW-EPR linewidth and we proposed a mechanism to explain the short T_1 [22].

Also for CIS1$^-$ one can notice a slight diminution of the linewidth on decreasing the temperature, as reported in Table 3, though this decrement is much less than for simple FP monoadducts in the same solvent: for instance, for NTEG$^-$ the peak to peak linewidth decreases from about $8 \times 10^6\,s^{-1}$ down to $3 \times 10^6\,s^{-1}$ in the range 260–160 K [22], while for CIS1$^-$ linewidth variations are between $1.4 \times 10^6\,s^{-1}$ and $1.0 \times 10^6\,s^{-1}$ in the same temperature range.

For CIS2$^-$ four species are visible in the X-band spectra and the analysis of the spectral profile is complicated. However, it is apparent that the linewidth trend is different for each species, as one can see

from the Table 4. Only the species with the highest *g*-factor, giving rise to the triplet at low field (species I), presents a line broadening on lowering temperature, as typical of "normal" low symmetry radicals. The other species, with lower *g*-factors, behave like typical fullerene derivative radicals, although linewidth variations are quite small. It is reasonable, on the basis of our model, that the four species are conformers of the CIS2 molecule in equilibrium and that the different linewidth trend relates to a different spin-density distribution and/or a different stiffness of the conformers. Accordingly, the species with the highest *g*-factor corresponds to a stiffer conformation. This is also in agreement with the *g*-factor analysis discussed previously.

Similarly, the lowest *g*-factor values in $CIS3^-$ spectra can be attributed to a flexible conformer, since the linewidth trend is a remarkable linewidth reduction on lowering the temperature, as typical for high symmetry fullerene derivative radicals.

5. Conclusions

This study has shown that in the low symmetry radicals we examined anomalous effects in the EPR linewidths are also present. Evidence is found that the increase in linewidths on increasing the temperature can be correlated with the lack of stiffness of the fullerene moiety.

The values of the ^{14}N hcc in the different compounds show that the spin-density distribution near the pyrrolidine ring is nearly the same in all the radicals. Moreover, in some cases the lack of any ^{14}N coupling indicates the presence of conformations with an axial nitrogen lone pair.

The values of the measured ^{13}C hcc have provided an indication of the symmetry of the spin-density distribution over the buckyball, that compares well with the molecular symmetry of the compounds.

The X-band spectra have shown that for compounds CIS2 and CIS3 the radical anions are present in different conformations in thermodynamic equilibrium. This is in agreement with the expectation that the methylene chain connecting the two rings would increase the energy barrier between them, in comparison with the FP mono and bisadducts.

For CIS1, the HF-EPR spectra results put in evidence different conformations. Comparing the X-band and W-band data we have been able to estimate the value for the interconversion rate between different CIS1 conformations. This dynamical information could only be obtained by measuring the EPR spectra at different frequencies and stresses the importance to use a multifrequency approach in order to investigate the dynamical behaviour of fullerene derivative radicals.

Acknowledgments

We thank Dr. Giancarlo Agostini for his valuable technical support, Mrs. Emanuela Zangirolami and Mrs. Sabrina Mattiolo for their help in the preparation of the radical anions. This work was supported by MURST (cofin prot. MM03198284) and by C.N.R. through the program "Materiali Innovativi (legge 95/95)."

References

[1] T. Kato, T. Kodama, M. Oyama, S. Okazaki, T. Shida, T. Nakagawa, Y. Matsui, S. Suzuki, H. Shiromaru, K. Yamauchi, Y. Achiba, Chem. Phys. Lett. 186 (1991) 35.
[2] P.M. Allemand, G. Srdanov, A. Koch, K. Khemani, F. Wudl, Y. Rubin, F. Diederich, M.M. Alvarez, S.J. Anz, R.L. Whetten, J. Am. Chem. Soc. 113 (1991) 2780.
[3] A. Penicaud, J. Hsu, C.A. Reed, A. Koch, K.C. Khemani, P.M. Allemand, F. Wudl, J. Am. Chem. Soc. 113 (1991) 6698.
[4] M. Rübsam, K.P. Dinse, M. Plüschau, J. Fink, W. Krätschmer, K. Fostiropoulos, C. Taliani, J. Am. Chem. Soc. 114 (1992) 10059.
[5] D. Dubois, M.T. Jones, K.M. Kadish, J. Am. Chem. Soc. 114 (1992) 6446.
[6] J. Stinchcombe, A. Pénicaud, P. Bhyrappa, P.D.W. Boyd, C.A. Reed, J. Am. Chem. Soc. 115 (1993) 5212.
[7] U. Becker, G. Denninger, V. Dyakonov, B. Gotschy, H. Klos, V. Rösler, A. Hirsh, H. Winter, Europhys. Lett. 21 (1993) 267.
[8] R. Subramanian, P. Boules, M.N. Vijayashree, F. D'Souza, M.T. Jones, K.M. Kadish, Chem. Commun. (1994) 1847.
[9] A. Stasko, V. Brezova, S. Biskupic, K.P. Dinse, P. Schweitzer, M. Baumgarten, J. Phys. Chem. 99 (1995) 8782.
[10] A. Stasko, V. Brezova, P. Rapta, K.D. Asmus, D.M. Guldi, Chem. Phys. Lett. 262 (1996) 233.
[11] M. Iyoda, S. Sasaki, M. Yoshida, Y. Kuwatani, S. Nagase, Tetrahedron Lett. 37 (1996) 7987.
[12] Y. Sun, T. Drovetskaya, R.D. Bolskar, R. Bau, P.D.W. Boyd, C.A. Reed, J. Org. Chem. 62 (1997) 3642.
[13] F. Arena, F. Bullo, F. Conti, C. Corvaja, M. Maggini, M. Prato, G. Scorrano, J. Am. Chem. Soc. 119 (1997) 789.
[14] V. Brezova, A. Stasko, P. Rapta, D.M. Guldi, K.D. Asmus, K.P. Dinse, Magn. Reson. Chem. 35 (1997) 795.
[15] S.A. Olsen, A.M. Bond, R.G. Compton, G. Lazarev, P.J. Mahon, F. Marke, C.L. Raston, V. Tedesco, R.D. Webster, J. Phys. Chem. A 102 (1998) 2641.
[16] C.A. Reed, R.D. Bolskar, Chem. Rev. 100 (2000) 1075.
[17] M. Maggini, G. Scorrano, M. Prato, J. Am. Chem. Soc. 115 (1993) 9798.
[18] M. Prato, M. Maggini, Acc. Chem. Res. 31 (1998) 519.
[19] M. Prato, J. Mater. Chem. 7 (1997) 1097.
[20] M. Prato, Fullerenes Relat. Struct. 199 (1999) 173–187.
[21] M. Brustolon, A. Zoleo, G. Agostini, M. Maggini, J. Phys. Chem. A 102 (1998) 6331.
[22] A. Zoleo, A.L. Maniero, M. Prato, M.G. Severin, L.C. Brunel, K. Kordatos, M. Brustolon, J. Phys. Chem. A 104 (2000) 9853.
[23] S.S. Eaton, A. Kee, R. Konda, R.G. Eaton, P.C. Trulove, R.T. Carlin, J. Phys. Chem. A 100 (1996) 6910.
[24] P.W. Atkins, D. Kivelson, J. Chem. Phys. 44 (1966) 169.
[25] T. Da Ros, M. Prato, V. Lucchini, J. Org. Chem. 65 (2000) 4289.

[26] K. Kordatos, S. Bosi, T. Da Ros, A. Zambon, V. Lucchini, M. Prato, J. Org. Chem. 66 (2001) 2802.
[27] A.K. Hassan, L.A. Pardi, J. Krzystek, A. Sienkiewicz, P. Goy, M. Rohrer, L.C. Brunel, J. Magn. Reson. 125 (1997) 207.
[28] M. Eiermann, R.C. Haddon, K. Brian, Q. Chan Li, M. Maggini, N. Martin, T. Ohno, M. Prato, T. Suzuki, F. Wudl, Angew. Chem. Int. Ed. 34 (1995) 159.
[29] B. Knight, N. Martin, T. Ohno, E. Ortí, C. Rovira, J.H. Veciana, J. Vidal-Ganced, P. Viruela, R. Viruela, F. Wudl, J. Am. Chem. Soc. 119 (1997) 9871.
[30] N.M. Atherton, Principle of Electron Spin Resonance, Ellis Horwood/PTR/Prentice-Hall, New York, 1993.
[31] A.J. Shell-Sorokin, F. Mehran, G.R. Eaton, S.S. Eaton, A. Viehbeck, T.R. O'Toole, C.A. Brown, Chem. Phys. Lett. 195 (1992) 225.